Interrogation of Oxidative Pulsed Methods for the Stabilization of Copper Electrodes for CO_2 Electrolysis

Kok, Jesse; de Ruiter, Jim; van der Stam, Ward; Burdyny, Thomas

DOI
10.1021/jacs.4c06284

Publication date
2024

Document Version
Final published version

Published in
Journal of the American Chemical Society

JACS
JOURNAL OF THE AMERICAN CHEMICAL SOCIETY
pubs.acs.org/JACS

Article

Interrogation of Oxidative Pulsed Methods for the Stabilization of Copper Electrodes for CO_2 Electrolysis

Jesse Kok, Jim de Ruiter, Ward van der Stam, and Thomas Burdyny*

Cite This: J. Am. Chem. Soc. 2024, 146, 19509−19520

Read Online

ACCESS | Metrics & More | Article Recommendations | Supporting Information

ABSTRACT: Using copper (Cu) as an electrocatalyst uniquely produces multicarbon products (C_{2+}-products) during the CO_2 reduction reaction (CO2RR). However, the CO2RR stability of Cu is presently 3 orders of magnitude shorter than required for commercial operation. One means of substantially increasing Cu catalyst lifetimes is through periodic oxidative processes, such as cathodic−anodic pulsing. Despite 100-fold improvements, these oxidative methods only delay, but do not circumvent, degradation. Here, we provide an interrogation of chemical and electrochemical Cu oxidative processes to identify the mechanistic processes leading to stable CO2RR through electrochemical and *in situ* Raman spectroscopy measurements. We first examine chemical oxidation using an open-circuit potential (OCP), identifying that copper oxidation is regulated by the transient behavior of the OCP curve and limited by the rate of the oxygen reduction reaction (ORR). Increasing O_2 flux to the cathode subsequently increased ORR rates, both extending lifetimes and reducing "off" times by 3-fold. In a separate approach, the formation of Cu_2O is achieved through electrochemical oxidation. Here, we establish the minimum electrode potentials required for fast Cu oxidation (−0.28 V *vs* Ag/AgCl, 1 M $KHCO_3$) by accounting for transient local pH changes and tracking oxidation charge transfer. Lastly, we performed a stability test resulting in a 20-fold increase in stable ethylene production *versus* the continuous case, finding that spatial copper migration is slowed but not mitigated by oxidative pulsing approaches alone.

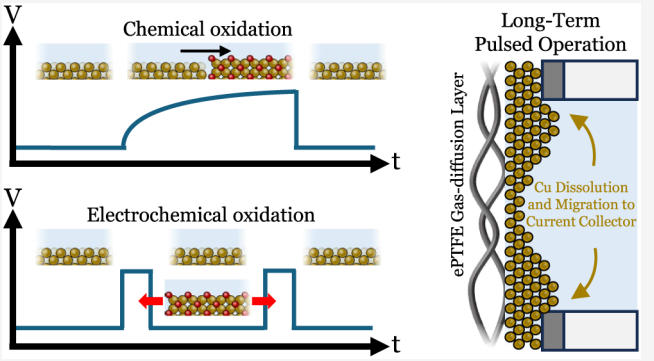

INTRODUCTION

With the use of electrical energy as an input, carbon dioxide (CO_2) can be converted to useful chemical compounds, enabling a more circular industrial carbon cycle.[1] One enabling technology is CO_2 electrolyzers which can form a bridge between renewable energy sources and the production of chemical feedstocks. The product species found at the outlet of CO_2 electrolyzers, however, depend on the cathode material used and the reaction medium.[2−4] Using copper (Cu) allows for the formation of multicarbon (C_{2+}) products, such as ethylene (C_2H_4), ethanol (C_2H_5OH), and acetate (CH_3COOH).[5] These products are desirable compounds given their market value and function in society.[6,7]

Electrochemical production methods, however, must be cost-competitive in order to flourish, placing an emphasis on performance metrics such as Cu product selectivity,[8−10] efficiency, current density, and stability. Increases in current densities have been enabled through the introduction of gas diffusion electrodes (GDEs),[11−13] while placing GDEs in a membrane electrode assembly (MEA)[14] allows for high energy efficiencies. Unfortunately, Cu stability acts as a major barrier to the commercialization of CO_2 electrolyzers, where operational time scales of >40,000 h of CO_2 reduction reaction (CO2RR) production are needed.[15] The Faradaic efficiency (FE) of C_2H_4 and other C_2-products for most lab-scale systems currently degrades within 10 h of operation due to a mixture of Cu catalyst degradation,[16−18] impurity deposition,[19,20] and salt formation.[21,22] Of these possible forms of failure mechanisms, the degradation of Cu is the most unresolved and severely hampers CO_2 electrolyzers.

In recent years, the degradation of Cu catalysts in near neutral media has been investigated more intensively, with a specific focus on the mechanisms resulting in structural deformations, also called restructuring. These mechanisms have been separately identified as oxidation-induced, electrolyte-induced, potential-induced, and carbon monoxide (CO) induced. For example, in the work by Raaijman *et al.*, Cu restructuring was shown to be a result of the initial reduction step of the copper oxide (Cu_xO) precatalyst to Cu upon applying a potential.[20] Further, when a Cu electrode is

Received: May 10, 2024
Revised: June 21, 2024
Accepted: June 24, 2024
Published: July 5, 2024

immersed in an electrolyte at the open circuit potential (OCP), the dissolution of Cu species can occur as an initial oxide layer forms.[23,24] These changes to the structural morphology were also observed using *in situ* atomic force microscopy.[18] Use of reducing potentials has been shown to, besides the dissolution and redeposition mechanism, induce Ostwald ripening, a phenomenon characterized by the growth of secondary particles.[25] This particle dissolution and coalescence mechanism is frequently described as the first restructuring mechanism found after an oxidation/reduction cycle. *In situ* Raman spectroscopy and fluorescence measurements have shown the partial dissolution of the Cu electrode to be in the form of a copper−carbonate hydroxide complex.[24,26−28] The carbonate ions within this complex allow for the direct formation of CO at low cathodic overpotentials.

With time, a transition from dissolution and coalescence into Ostwald ripening[29,30] leads to a broadening of the particle size distribution. The migration of dissolved copper complexes is made possible here due to a local alkaline environment, where the presence of local OH^- ions has been shown to induce autonomous oxidation/redeposition reactions involving the metallic Cu species.[31] In addition, cathodic corrosion could explain the migration of dissolved Cu complexes, similar to platinum.[32] This mechanism was found to be the main cause of the deteriorating catalyst performance during cathodic polarization on the Cu catalyst, in both argon and CO environments.[33] Here, nanofragments were formed during the reduction reactions and resulted in an increased CO_{bridge}/CO_{atop} (spatiotemporal-resolved *in situ* Raman spectroscopy) ratio that poisoned the catalyst surface. Without removal of poisoned sites *via* methods such as pulsing, the catalytic selectivity to the desired products degrades. Despite the many proposed ways in which copper dissolves and redeposits over time, there is a consensus in the field that Cu restructuring in general is responsible for the loss of CO_2 reduction selectivity, especially to C_{2+} compounds.

Although surface restructuring can be the dominant catalyst degradation pathway, the other possible failure mechanisms should not be excluded immediately. When a system is predominantly suffering from flooding or salt formation, it can be easily tracked through ECSA calculations, changing the local CO_2 concentration or simply by studying the GDE post-operation. Evaluating the possibility of impurity deposition is more challenging. Impurities originating from the system materials or electrolyte salts, such as Fe, Zn, or Pb, can be reduced on the cathode electrode during electrolysis. As a result, the system can start showing an increase in the activity for the hydrogen evolution reaction (HER) over CO2RR.[34] This results in a selectivity change over time, although the characteristics of the changes are different than when Cu restructuring is described as the main cause of catalyst degradation. Studies that exclude impurity deposition as a possible degradation do frequently so by showing the purity of the electrode using X-ray photoelectron spectroscopy (XPS). It can be an excellent method to study the top 0.5−2 nm surface composition, but as the catalyst layer is often in the order of 100 nm, there is a likelihood that the metallic impurities are present beyond the 2 nm detection limit of XPS.[33]

Electrochemical systems suffering from limited stability caused by the deposition of metallic impurities during reductive phases frequently have a low geometric cathode area to catholyte volume ratio in combination with a low roughness factor of the cathode catalyst.[19] These systems often show decay in the FEs of CO2RR products within 10 min of applying a reductive current or potential. Chemically purifying the electrolyte, for example with ethylenediaminetetraacetic acid (EDTA), has been shown to increase the catalyst lifetime in multiple works and can be an excellent way to show how much the catalyst lifetime is affected by present impurities.[34,35] Only by detailed evaluation of the FE trends of the CO2RR products and of the Cu electrode structure post-operation, failure mechanisms can be characterized as a main or minor contributor to the limited catalyst lifetime at different time scales.

In efforts to counteract Cu restructuring and "reset" a Cu electrode system during operation, pulsed electrolysis has been put forward as a method to achieve stable CO_2 reduction.[36−38] During pulsed electrolysis, the applied Cu electrode voltage is periodically varied between CO_2 reducing potentials and more anodic potentials capable of passivating Cu to Cu_xO. The formation of an oxide layer in the more anodic pulse, for example cuprite (Cu_2O), is shown to revive the electrocatalytic activity toward C_2 product formation during the cathodic pulse.[38−40] The reasons for C_{2+} product regeneration are heavily debated. For example, some works state that reducing the Cu_2O to oxide-derived copper (OD-Cu) leads to increased density of grain boundaries and surface defects, promoting the formation of C_2 products like C_2H_5OH or C_2H_4.[9] Other works, such as the work from Xiao *et al.*, suggest that the promoted electrochemical activity of OD-Cu originates from simultaneously present metallic copper (Cu^0) and oxidized copper (Cu^+) under reducing conditions.[41,42] However, these statements have frequently been discredited by other scientific works using electron energy loss spectroscopy and XPS as these show no Cu^+ species to remain present during CO2RR. Notably, the thermodynamic energy barrier for the reduction of Cu^+ to Cu^0 is lower than that required to perform CO2RR, and beyond subsecond time scales at reducing potentials all oxide species should be reduced.[43,44]

As an added complexity, pulsed operation can be applied in numerous ways to form Cu passivation layers, with each approach impacting product selectivity and stability differently. Work from Obasanjo *et al.* set the Cu electrode as an anode, using oxidative currents to electrochemically form Cu_xO.[36] Conversely, Nguyen *et al.* utilized 15 min periods of OCP to achieve chemical oxidation of a catalyst deposited onto a GDE, which also renewed the cathode's activity toward C_2H_4.[37] In both of the above-described works, *in situ* Raman spectroscopy showed the formation of Cu_xO when the cathode was exposed to oxidation charges or the OCP.

The improved stability was attributed to the formation of these oxides through both the electrochemical and chemical oxidation steps *via* pulsed operation, but the impacts of precise anodic potentials, the effects of local pH, and chemical oxidation rates can all be varied to give different copper stabilities.

More importantly, while pulsing has shown the ability to increase catalyst lifetimes, activity is still shown to steadily degrade over longer time scales. Thus, net restructuring is either still happening even with pulsed operation, or long operation reveals a previously uninvestigated separate degradation pathway. Greater knowledge and contextualization on the chemical processes involved in pulsed electrolysis for extending catalyst lifetime are a necessity to understand and extend Cu catalyst lifetimes.

https://doi.org/10.1021/jacs.4c06284
J. Am. Chem. Soc. 2024, 146, 19509−19520

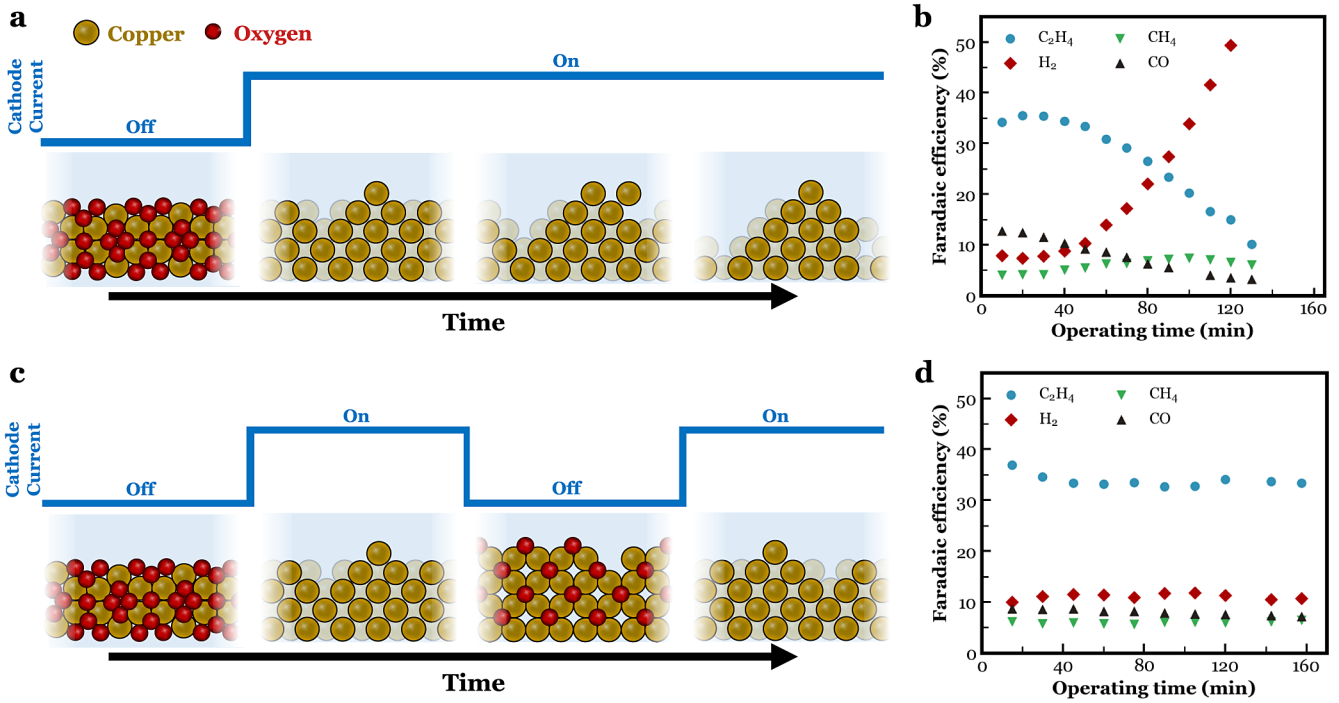

Figure 1. (a) Current profile during a constant chronopotentiometry experiment at -100 mA · cm^{-2} along with schematics illustrating the changes in chemical state and morphology at the different stages of the experiment. (b) FE curves of C_2H_4, CO, CH_4, and H_2 as a function of operating time during the experiment depicted in (a). (c) Current profile during pulsed CO_2 electrolysis where a reductive current at -100 mA · cm^{-2} was alternated with an oxidative pulse. (d) FE curves of C_2H_4, CO, CH_4, and H_2 as a function of operating time during the experiment depicted in (c). Here, 15 min at -100 mA · cm^{-2} was followed by 15 min at OCP.

Within this work, we provide context and the underlying chemical conditions governing copper oxidation processes during pulsed electrolysis to maintain the catalyst's activity toward C_2 product formation through a combination of electrochemical and *in situ* Raman spectroscopic measurements. We examine both chemical and electrochemical oxidation processes which generate Cu_2O to formulate the different criteria necessary to extend C_2H_4 production from CO_2 electrolysis. By examining oxidation potential, time, and charge, we define the half reactions occurring and the minimum required anodic pulse time. With the formulated criteria, a stability test was designed reaching 18 h of CO_2 electrolysis with a minimal drop in the FE of C_2H_4 under realistic reaction conditions.

RESULTS AND DISCUSSION

In this work, for all experiments unless stated otherwise, we used a 300 nm Cu catalyst layer sputtered onto a polytetrafluoroethylene (PTFE) GDE and operated in a PEEK-flow cell with a flowing catholyte. Using the flowing catholyte and a PTFE GDE avoids both salt formation and flooding instabilities in all tests allowing for the catalyst stability to be assessed individually on the basis of Cu restructuring. Further, no pretreatments or roughening have been done to the sputtered Cu, which oxidizes to copper(II) oxide (CuO) after exposure to air after deposition. A 1 M $KHCO_3$ catholyte was also chosen for these experiments as this represents a stable CO_2 electrolyzer configuration as compared to alkaline electrolytes. Notably, Cu catalysts are significantly more stable in higher pH electrolytes, but the use of a neutral-pH electrolyte is more representative of future applications. The PTFE sputtered Cu GDE (Figure S1), and all the details of the setup are found in Figures S2 and S3.

Using the above-described setup, we first wanted a continuous operation baseline (Figure 1a) with no pulsing as a benchmark to evaluate Cu stability. We chose a fixed current density of -100 mA·cm^{-2} and operated in chronopotentiometry mode, with the measured potential given in Figure S4. The gas FEs were measured during operation with a gas chromatograph (GC). Here, we will primarily use the C_2H_4 FE as a criterion for stability. While the selectivity of hydrogen (H_2), methane (CH_4), and CO also shows particular trends during degradation and adds further dimensions to the analysis, as the desired target product for the reaction, we will focus primarily on C_2H_4 as a stability descriptor. As shown in Figure 1b, while the C_2H_4 FE starts at 35%, there is a rapid decay within 1 h operation. Followed by an increase in H_2 as was found to be consistent with other works.[36−38] It is worth noting that these C_2H_4 FEs can likely be increased up to 40−50% by roughening, using higher current densities or a higher pH as shown elsewhere, but this was not a focus of the work. As a negative current was applied, the Cu is believed to initiate a restructuring response[45] as the change in chemical state from Cu^+ to Cu^0 forces the material to take up a new unit cell. The high number of uncoordinated atoms at the surface can result in a significant amount of surface defects with this sudden change in the crystal lattice.[46] The restructuring was studied using *ex situ* SEM analysis (see Figure S5). SEM images show a more agglomerative and dense structure at the sides of the GDE as well as large needlelike structures.[23,29,47,48] The CO2RR gas product selectivity curves of three independent experiments continuously operated at current density of 100 mA · cm^{-2} are plotted in Figure S6. The time evolution of

https://doi.org/10.1021/jacs.4c06284
J. Am. Chem. Soc. 2024, 146, 19509−19520

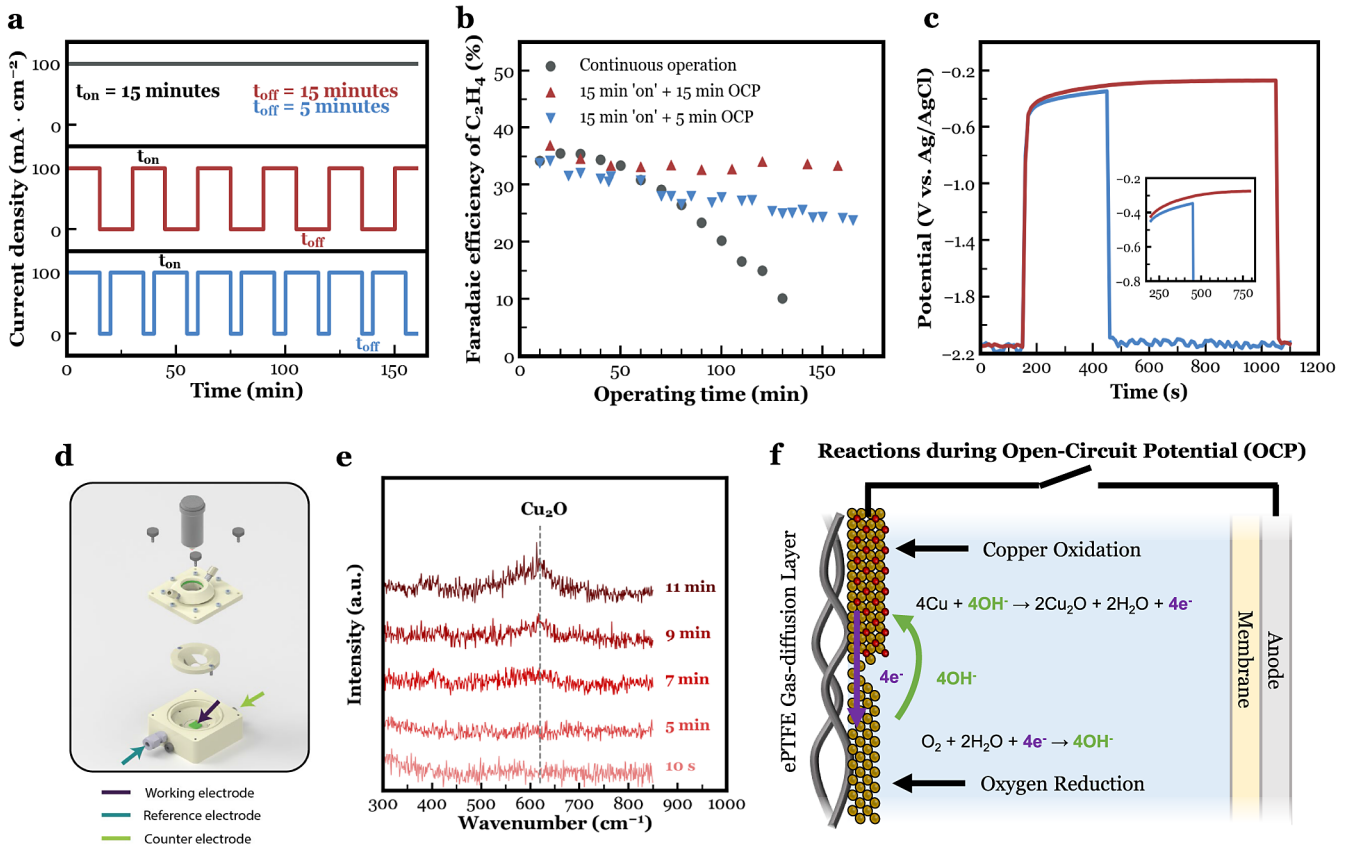

Figure 2. (a) The different performed chronopotentiometry experiments. A constant current density at −100 mA·cm^{-2} (black). A pulsed current with 15 min at −100 mA·cm^{-2}, followed by 15 min at OCP (red). A pulsed current with 15 min at −100 mA·cm^{-2}, followed by 5 min at OCP (blue). (b) FE of C_2H_4 as a function of time for the current profiles depicted in (a). (c) Change in OCP value with time during the oxidative pulse. (d) The *in situ* Raman spectroscopy setup. (e) Raman spectroscopy data showing the intensity of the Cu_2O signal at different OCP times. (f) The half reactions associated with the formation of Cu_2O during OCP.

other products can provide additional information on the nature of the catalyst. After 1 h, the FE curves of C_2H_4 and CO experience a decay, whereas the activity of the Cu GDE toward CH_4 and H_2 increases. The increase in CH_4 is especially more noticeable at a higher number of operational hours. Comparing Figures S2 and S5, it becomes clear that the electrode underwent a restructuring change as a result of early dissolution and redeposition and Ostwald ripening. With operating time, the spherical-like particles (Figure S2) were converted into smaller cubic structures (Figure S5a) at the center of the GDE. The perimeter of the GDE shows, in comparison to the center, a much more agglomerated dense structure (Figure S5b). A difference in Cu structure has been correlated with different CO2RR product activities.[49]

We speculate the difference in morphology between the center and perimeter of the Cu GDE to be the result of the uneven potential distribution across the GDE, resulting in directional migration of dissolved and redeposited species.

Looking at our continuous operation benchmark, we then wanted to confirm that other failure modes (impurity deposition, salt formation, and flooding) were not dominant on these time scales. Some conclusions can be taken from the selectivity trends displayed in Figure S6. As deposited metallic impurities should suppress the formation of all hydrocarbons, impurity deposition is not likely to be a dominating factor in the observed results. This is to be expected as the geometric area of the electrode−to−catholyte volume ratio of our electrochemical cell (2 cm^{-1}), the roughness factor of the used GDE (>12) as determined by an ECSA analysis (Figure S7 and Table S2), and the time scale of the observed change in selectivity all suggest the impurity deposition to be a less plausible explanation of our results. As a confirmatory analysis, with energy-dispersive X-ray spectroscopy (EDS), no metallic impurities were found to accumulate on the catalyst surface within the detection limits of the technique (Figure S8 and Table S3).

Furthermore, no salt particles were found on the GDE after the test (Figure S9). Hence, the observed trend of product selectivity is attributed to the morphology and chemical state change of copper with operating time.

We also assessed the comparable rate of C_2H_4 decay as a function of catalyst layer thickness, applied current density, and catholyte pH (Figures S10−S12) all of which will impact the amount of Cu restructuring and the stability during operation. The results show a clear relation between catalyst layer thickness and stability, with thicker catalyst maintaining higher stability during operation. Although a higher current density proved to be detrimental in terms of stability for a thin Cu layer (100 nm), thicker catalyst appeared to show improved stability and starting FE of C_2H_4 with increasing current density in the first operational hour. These improvements in performance metrics are suspected to be a result of the increase in local pH with higher current densities as this is known to suppress HER.[50] However, going beyond a certain current density does not pay back with improved stability. Similarly, utilizing a higher pH catholyte, for example 0.5 M K_2CO_3 (pH

https://doi.org/10.1021/jacs.4c06284
J. Am. Chem. Soc. 2024, 146, 19509−19520

= 12), resulted in both a more stable and more selective C_2H_4 production as compared to the 1 M $KHCO_3$ catholyte (pH = 8.3). Understanding the effect of the above evaluated parameters on the lifetime of Cu catalyst allows for the design of an experimental setup that can assess the stability in a low number of operational hours.

As discussed before, (electro)chemical oxidation can be periodically implemented to stabilize the FE of C_2H_4 and prevent the HER from becoming more dominant. A general illustration of these pulsed experiments is shown in Figure 1c. Here, we fixated the current density of the pulsed experiments at a reductive current density of -100 mA · cm^{-2}, while varying the conditions of the oxidative pulse. During the oxidative pulse, the voltage on the Cu electrode is more anodic and can therefore result in the oxidation of Cu to Cu_2O depending on the local pH and applied potential as prescribed by the Pourbaix diagram.[51] An oxidative pulse can be done in two ways (i) either through setting the cathode to OCP resulting in chemical oxidation or (ii) by actively setting the Cu electrode as an anode and applying an oxidative current, resulting in electrochemical Cu oxidation. During pulsed operation, the length and potentials of the reductive pulses and oxidative pulses were controlled by a potentiostat. The effect of incorporating oxidation phases is shown in an initial experiment in Figure 1d. Here, a pulsed operation was applied where 15 min of operation at -100 mA · cm^{-2} ("on" time) was followed by 15 min of OCP ("off" time). These cycles then continued for a total CO_2 reduction operating time (*e.g.*, time spend at -100 mA · cm^{-2}) of 157 min. The potential during operation remained close to -2.2 V *vs* Ag/AgCl for both the continuous and pulsed operation in Figure 1 as shown in Figures S4 and S13. As shown in Figure 1d, a 3% drop in the FE of C_2H_4 was observed for the pulsed operation providing a stark contrast *versus* the continuous operation case (Figure 1a,b). These combined results then provide a baseline to further evaluate the effect of copper oxidation processes.

Chemical Oxidation. With chemical oxidation established to extend Cu lifetimes as elsewhere,[37] we sought to resolve the chemistry governing the oxidation process and the time-resolved growth of the oxide layers. In particular, we performed an electrochemical analysis of the Cu electrode under various "off" times to assess the importance of "off" time on Cu oxidation and C_2H_4 stability. Further, we examine how the addition of oxygen influences the cathode voltage during these "off" periods and cathode stability as this method has been previously utilized to lengthen catalyst lifetimes.[37]

As shown in Figure 2a, three scenarios were compared including continuous and pulsed operation, with OCP set during the anodic pulse. Here, the "on" times were fixed at 15 min, while the OCP periods were held at 15 and 5 min (Figures S13 and S14). When looking at the measured FE of C_2H_4 as a function of operating time in Figure 2b, we can see 5-min OCP periods are an improvement over the continuous case, but less stable than 15-min OCP periods which maintained most of the starting C_2H_4 FE after 157 min of operating time. The FEs of all the gas products are included in Figure S15. From these findings, it can be determined that chemical oxidation is a slow process, and that 5 min is insufficient to fully oxidize the entire Cu catalyst layer, although partial oxidation is occurring.

Despite the differences in the FE curves of C_2H_4 in Figure 2b, morphological changes can be observed to all three GDE samples as shown by the *ex situ* SEM images in Figures S5 and S16. The microneedles observed in the latter figure can be attributed to the formation of copper hydroxide ($Cu(OH)_2$).[52,53] These nanowires form as a consequence of Cu dissolving shortly before the passivation layer is formed.[48]

As confirmation that the OCP periods can also regenerate the activity of the Cu catalyst after the C_2H_4 selectivity decreased, we also performed experiments using longer reduction times of 1 h instead of the 15 min in Figure 2b. These results, shown in Figure S17, illustrate that a 15-min OCP period can recover catalyst activity.

To understand the relation between the programmed OCP time and Cu stability, we can look at the half reactions occurring on the cathode and track the electrochemical potential during OCP. There is no complete electrochemical circuit during OCP, meaning the cathode potential will equilibrate according to the electrode−electrolyte interface. Under these conditions upon turning the potentiostat off, the cathode potential will drop from the applied potential of -2.2 V *vs* Ag/AgCl to -0.5 V *vs* Ag/AgCl within 1 s (Figure 2c). This process is regulated by the capacitive discharge. After spending 15 min at OCP, the OCP approaches the thermodynamic value for a Cu electrode surface located in a 1 M $KHCO_3$ solution (-0.27 V *vs* Ag/AgCl). The red curve (Figure 2c) stabilizes at this value, whereas spending only 5 min at OCP did not allow this to happen. Stabilization occurs close to a potential window where, as described by the Pourbaix diagram of our catalyst, Cu_2O starts to become the thermodynamically most stable state.[51] As 15 min at OCP allowed for more time to be spend in this potential window, more Cu is expected to become activated through oxidation/reduction cycles as compared to spending 5 min at OCP. Accordingly, the latter resulted in a mixed active/inactive CO_2 electrocatalyst as indicated by the steadily decaying FE of C_2H_4 over time (Figure 2b), but one that is still more stable than the continuous case.

In situ Raman spectroscopy was then used to understand the correlation between the plotted OCP curves in Figure 2c and the catalyst lifetime as depicted in Figure 2b. The *in situ* Raman spectroscopy setup used for this purpose is shown in Figure 2d. The setup is explained in more detail in Supporting Information (see In Situ Raman Spectroscopy section). The Cu electrode used to perform Raman spectroscopy measurements differed from those used during electrochemical measurements. Formation of Cu_2O was studied as a function of both potential and time by measuring Raman signals characteristic for the presence of Cu_2O. Figure 2e shows a Raman signal at a wavenumber of 630 cm^{-1}, one that can be assigned to Cu_2O, after roughly 9 min of "off" time, which can be assigned to Cu_2O. In literature, Raman spectra of Cu_2O electrodes display three distinct features at 390, 520, and 630 cm^{-1}, ascribed to (partially) Raman-allowed lattice vibrations.[28] The 630 cm^{-1} feature (ascribed to defects in the Cu_2O lattice) is the most intense vibrational band for Cu_2O, and the signal-to-noise ratio of the current measurements only allows identification of this characteristic Cu_2O band. The Raman data together with the OCP curves explain that the oxidation of Cu to Cu_2O is not initiated immediately after switching from a reductive current density to OCP. Instead, some time is required for the properties of the local environment to equilibrate back to the bulk environment. This change then allows for the OCP to transient back to a potential that falls within the borders of the Cu_2O region of the Pourbaix diagram.[51] In other words, the fraction of the OCP period

https://doi.org/10.1021/jacs.4c06284
J. Am. Chem. Soc. 2024, 146, 19509−19520

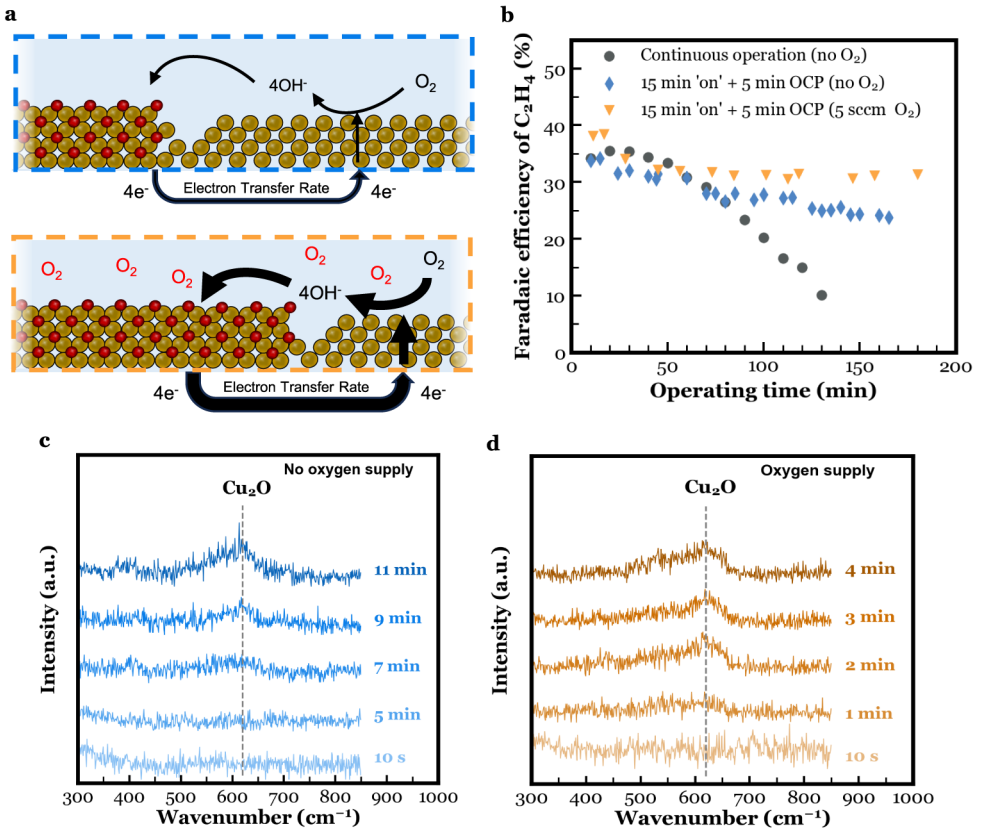

Figure 3. (a) A schematic illustrating the electron transfer between the copper oxidation reaction and the oxygen reduction reaction across the Cu electrode/electrolyte interface. The effect of a low (blue) or high (orange) oxygen flux to the cathode on the rate of the Cu_2O formation is shown. (b) FE of C_2H_4 as a function of operating time for a continuous operation and the two pulsed electrolysis experiments shown in (a). Raman signal plotted between 300 and 850 cm^{-1} at different OCP times without (c) and with (d) added oxygen supply.

during which the chemical oxidation of Cu is set to take place is largely determined by the transient behavior of the OCP curve.

Within a certain OCP potential range of Figure 2c, Cu oxidation is then continuously occurring (eq 1 below). This oxidation requires sufficient time and is expected to require an oxygen source in the form of hydroxide. These hydroxides conveniently come from the oxygen reduction reaction (ORR) which also occurs during the OCP period and is given by eq 2. Although water reduction could also act as a supplier of these hydroxides, we decided to focus on the reaction that is thermodynamically the most favorable to occur, which is ORR. ORR requires electrons, which are no longer provided by the anode during open-circuit operation. The necessary electron exchange then takes place across the cathode/electrolyte interface where the electrons are provided by the Cu oxidation reaction. Thus, the Cu electrode has simultaneous oxygen reduction and Cu oxidation spatially occurring on the same electrode when oxygen is present in the electrolyte (Figure 2f), and over time will result in full oxidation of Cu as long as sufficient oxygen is available. The process then becomes self-limiting once Cu is fully passivated or oxygen is depleted.

The two half reactions responsible for passivating the Cu electrode, along with the total reaction, are shown in eqs 1−3.[54−56]

$$2Cu + 2OH^- \rightarrow Cu_2O + H_2O + 2e^- \quad E_{red} = 0.265 - 0.059\cdot pH \quad (vs\ Ag/AgCl\ 3.5\ M\ KCl) \qquad (1)$$

$$O_2 + 2H_2O + 4e^- \rightarrow 4OH^- \quad E_{red} = 1.03 - 0.059\cdot pH \quad (vs\ Ag/AgCl\ 3.5\ M\ KCl) \qquad (2)$$

$$4Cu + O_2 \rightarrow 2Cu_2O \qquad (3)$$

We note that the equations above are formulated for neutral and alkaline media specifically. In more acidic environments, the half reactions exchange water molecules and electrons, not hydroxides.

Prior to Cu_2O formation, Cu dissolves at OCP.[29] Using ICP-MS, it was found that for every minute at OCP, 0.5% of the initial present mass is lost due to dissolution (Table S4). Thus, an increased number of oxidation and reduction cycles and increased time spent at OCP lead to more structural deformations that impact stable C_2H_4 production.[20] A sufficient amount of dissolved Cu is necessary before Cu_2O becomes the thermodynamically most stable state at the bulk pH (8.3) as given by the Pourbaix diagrams for different local Cu concentrations.[51]

To reduce time spent at OCP, it is desired to accelerate full Cu oxidation. Given the hydroxide ion and electron dependency between the two half reactions, the reaction rates of both processes can be controlled by the supply of reactants (Figure 3a). The change in the rate of Cu_2O formation and the OCP value can then be understood on a fundamental level using Evans (or mixed potential) diagram.[51,57]

Specifically, Cu_2O formation is a corrosion process and can be described by the intersection of the anodic and cathodic polarization curves of the reactions in eqs 1 and 2, respectively,

https://doi.org/10.1021/jacs.4c06284
J. Am. Chem. Soc. 2024, 146, 19509−19520

inside an Evans diagram. The construction of an Evans diagram can help understand the effect of reactant supply to the cathode on the chemical oxidation kinetics. We produced an anodic polarization curve of the Cu electrode by performing a linear sweep voltammetry from −0.4 to 0.3 V *vs* OCP at 20 mV/s (Figure S18). This potential sweep was chosen to first remove the already existing oxide layer. Cu oxidation then initiates at −0.28 V *vs* Ag/AgCl, and a maximum oxidation current is reached at 0.0 V *vs* Ag/AgCl. The 15-min OCP curve starts to flatten out near −0.28 V *vs* Ag/AgCl, further confirming the dependency of chemical oxidation on the transient behavior of the OCP curve. The expected cathodic polarization curve of the ORR is studied from literature and is expected to look similar to that depicted in Figure S19. Produced oxygen at the anode side that crossed over the membrane to the cathode and the little oxygen content of the catholyte are both the sources of the oxygen consumed by eq 2.

Figure S20 then shows the expected Evans diagram extracted from Figures S18 and S19. In Figure S21, the effect of increasing the oxygen content is visualized. The red line represents an anodic polarization curve for Cu oxidation, while the cathodic polarization curves are shown for a "low" (blue line) and "high" (yellow line) cathode oxygen content scenario. The plateau in the cathodic polarization curve is the limiting current density and is dependent on the oxygen availability (Figure S19). Thus, a greater oxygen presence will shift the cathodic polarization curve up and cause the intersection point of the ORR and Cu oxidation to move to higher rates (*y*-axis coordinate) and a more positive OCP (*x*-axis coordinate).[57−59] With this positive shift in OCP, increased oxygen pressure in the cathode compartment allows the OCP after a reductive current density to transient back quicker to a potential at which Cu_2O formation is allowed (Figure S18). With this in mind, the potential at which Cu starts to chemically oxidize to Cu_2O is theoretically met faster with the increased oxygen pressure.

We can then conclude that the amount of reactivated Cu in a given anodic time frame is limited by the O_2 content in the cathode compartment (Figure S20), which likely stems from crossover from the anolyte chamber through the membrane. To better understand these effects and shorten the required OCP time, we then performed the 5-min OCP experiment again (Figure 2a), but this time with oxygen supplied to the catholyte's headspace at a rate of 5 sccm throughout the entirety of the experiment (Figure S22).

As shown in Figure 3b, we can then see that under a supply of oxygen, a 5-min OCP period is then sufficient to maintain the FE of C_2H_4 as compared to the scenario without added O_2 to the catholyte. After 40 min of CO2RR, the FE of C_2H_4 stabilized at 30% and remained close to this value for another 140 min of operation. Thus, the chemical oxidation process was accelerated with the additional oxygen supply, resulting in a higher amount of Cu_2O after 5 min at OCP compared to when no additional oxygen was supplied. By observing the measured cathode potential over time during OCP (Figure S22c), we can see a quicker thermodynamic stabilization toward the passivated Cu_2O potential of −0.27 V *vs* Ag/AgCl. This positive shift in OCP is also expected based of the insights from the Evans diagram as shown in Figure S21.

The accelerated process of chemical oxidation with an elevated oxygen content at the cathode is further confirmed with *in situ* Raman spectroscopy data in Figure 3c,d. Here, the Raman signal between 300 and 850 cm^{-1} is plotted for different OCP times· The spectroscopy data verify that higher oxygen content near the Cu GDE significantly reduces the minimal required OCP time to start oxidizing Cu to Cu_2O. Then, the oxygen-filled Raman setup detected the presence of Cu_2O after less than 2 min at OCP. This duration is substantially shorter than the comparable case without added oxygen (∼7 min). Figure S23 shows Raman spectroscopy heatmaps where the Raman signal intensity is plotted as a continuous function of both time and wavenumber.

From eqs 1 and 2, it is also apparent that the measured OCP value is local pH dependent. This further explains the direction of the curves in Figure 2c. Beyond the potential jump regulated by capacitive discharge, the OCP curve is a result of the local pH equilibrating back to that of the bulk value.[59] With the local environment becoming less alkaline with time, the equilibrium potentials of eqs 1 and 2 become more positive. Accordingly, the *x*-coordinate intersection of the polarization curves, the OCP value, becomes more positive with time. The flattening of the OCP curve indicates the local pH is then equal to bulk pH. This, in combination with the previously results, suggests that the fraction of the OCP period during which the chemical oxidation of Cu is set to take place is largely determined by what rate the local pH drops back to the bulk value. The relation between OCP curve, local pH, and growth of Cu_2O is also schematically explained in Figure S24 using *in situ* Raman spectroscopy data.

In order to further demonstrate the effect of the change in local pH to the measured OCP value, a 1-h CO2RR experiment was performed in 0.5 M K_2CO_3 catholyte, followed by 5 min at OCP while recording the potential as a function of time (Figure S25). A lower increase in local pH during CO2RR is expected to occur when using K_2CO_3 as compared to $KHCO_3$, meaning equilibration to the bulk pH should occur notably quicker for the former electrolyte. The difference between local pH and bulk pH is then plotted as a function of OCP time for both electrolytes in Figure S26. Figures S25 and S26 show the flattening of the OCP curve to occur as the local pH approaches the bulk pH.

The observations made in this section provide insights in the chemical processes that take place during OCP, how OCP can be utilized to increase the catalyst lifetime and how the variance of different parameters can alter the required "off" time. This "off" time is aimed to be minimized to both increase the capacity factor of the overall process and to reduce the loss of catalyst mass through dissolution at OCP. Further, by monitoring the OCP, the progress of Cu oxidation can be tracked during each "off" period. Interestingly, the requirement for O_2 as a source of Cu oxidation also has implications for the usefulness of this pulsing approach. For example, in larger-scale systems where oxygen crossover across the membrane is either limited or may have spatial variations, it may be hard to guarantee full periodic oxidation of Cu catalysts without substantial "off" periods. These complications motivate more active or controllable Cu oxidation processes such as electrochemical routes in the next section.

Electrochemical Oxidation. A different means of oxidizing Cu is through the use of oxidative currents as a result of setting the Cu electrode as an anode and withdrawing electrons. As a closed electrochemical circuit exists, this method is an electrochemical oxidation approach, but similarly results in the formation of Cu_xO just like with chemical oxidation. However, the closed electrochemical circuit removes

https://doi.org/10.1021/jacs.4c06284
J. Am. Chem. Soc. 2024, 146, 19509−19520

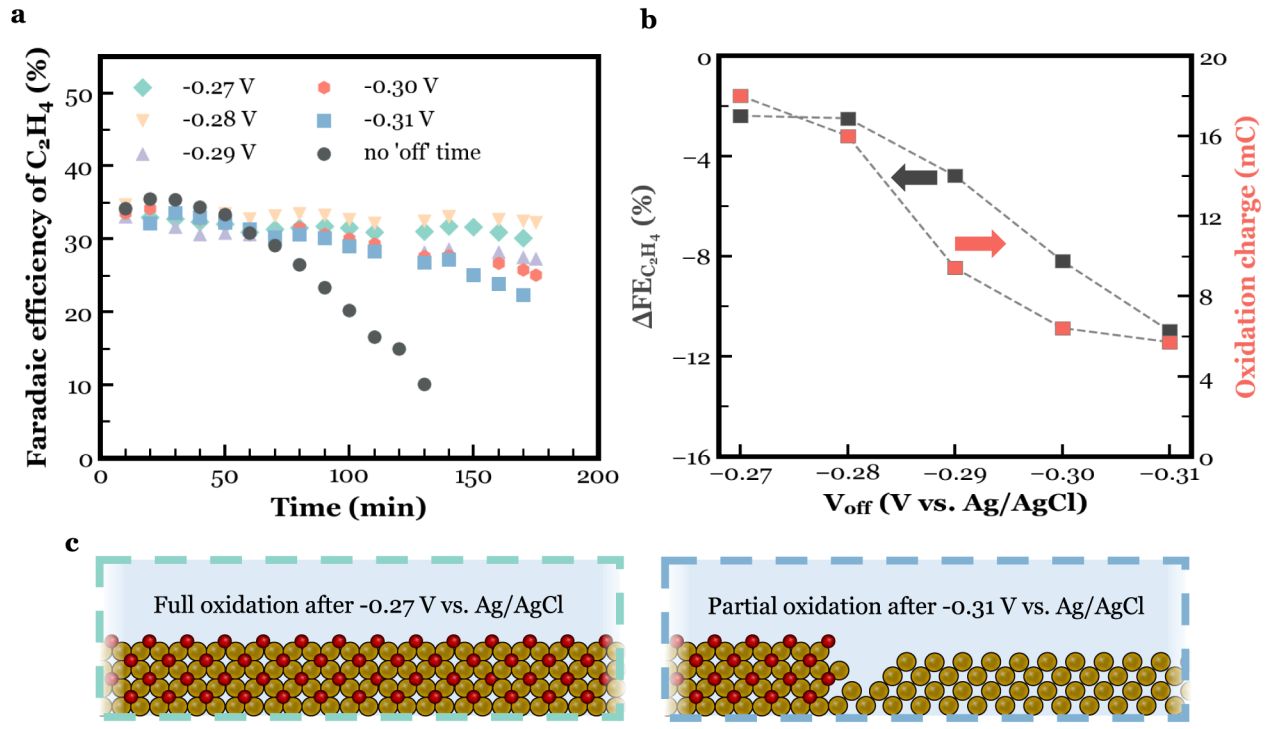

Figure 4. (a) The FE of C_2H_4 as a function of operating time for different "off" potential values (*vs* Ag/AgCl) during pulsed electrolysis. (b) The decay in the FE of C_2H_4 after 140 min of operating time (black) and the oxidation charge (red) as a function of programmed "off" potential. (c) Schematic picture showing the difference in Cu_2O growth at two oxidation potentials.

the necessity of consuming the liberated electrons by the ORR. Similar to the previous section, the Cu catalysts can be cycled through reduction and oxidative pulses to periodically recover CO_2 reduction selectivity toward products such as C_2H_4. Despite achieving the same goal of oxidizing Cu, the chemical and electrochemical oxidation processes will impact Cu restructuring and stability differently. Here, we contrast the electrochemical oxidative processes. As the previous section showed the number of oxidized Cu particles to be an important parameter in stabilizing CO_2 reduction through varying the length of the OCP period and oxygen levels, the same was believed to uphold for electrochemical oxidation with regards to potential. To assess this, CO2RR was performed for an hour at a reductive current density of -100 mA·cm^{-2}, followed by 30 s at various "off" potentials ranging from -0.27 to -0.31 V *vs* Ag/AgCl (Figure S27a). These potentials fall within the measured OCP range in the previous section. These cathodic and anodic cycles were repeated for a total operating time of 3 h. In these experiments, however, the flow of electrons between the anode and cathode is not restrictive, and the oxidative current on the Cu electrode can be measured using the potentiostat (Figure S27b).

The FE of C_2H_4 as a function of operating time for these various potential tests is shown in Figure 4a. Although only a minor difference of 10 mV between the oxidating potentials existed, differences in the effect on the catalyst lifetime were clearly visible (see Figure S28 for all gaseous products). In all cases, despite minor reduction in the ethylene FEs, a clear increase in H_2 is seen in all cases after 1 h of operation. This indicates that for this pulsed approach, an operating time of 1 h using a 300 nm thick Cu layer is too long and will negatively impact CO2RR product formation overall.

More information can also be gained by observing the measured current during the electrochemical oxidation process at various potentials. As shown in Figure S27b, for each of the anodic potential steps there is a decaying current curve over time from which a sampled-current voltammogram can be derived.[60] These current measurements can be analyzed to define the total accumulated charge (Figure 4b, red), which represents the total electrons withdrawn from the Cu electrode at each oxidation potential. When plotting the decay in the FE of C_2H_4 after 140 min of operation *versus* the total oxidative charge passed, there is a clear correlation (Figure 4b, black). These results indicate that a set potential of at least -0.28 V *vs* Ag/AgCl is required to sufficiently oxidize the entirety of the Cu electrode requiring a charge of roughly 16 mC for the electrode area and morphology. Potentials more negative than this value resulted in a lower FE of C_2H_4 after the three operational hours (Figure S27d). Interestingly, however, every "off" potential did result in a measured oxidation charge as shown in Figure 4c.

Potentially, similar to chemical oxidation, the degree to which the catalyst activity is maintained depends on the number of oxidized Cu particles during the oxidation periods. With the "off" potentials becoming more anodic, the measured oxidation charge increased, oxidation charge is proportional to the extent of passivation as illustrated in Figure 4d. Hence, the difference in the observed Cu catalyst lifetime with different applied oxidation potentials could be correlated, similar to chemical oxidation, to the degree to which Cu was oxidized.

Another possible reason for the detection of oxidation charge but a lack of C_2H_4 production stability with time would be the local pH effect on the stability of the different chemical states of Cu. Right after a reductive phase, the high local alkalinity would allow the Cu layer to oxidize even at potentials more cathodic than the -0.28 V *vs* Ag/AgCl which was based on the bulk pH. As the activity of CO2RR dropped to zero during this anodic phase and the oxidation reaction of Cu

https://doi.org/10.1021/jacs.4c06284
J. Am. Chem. Soc. 2024, 146, 19509−19520

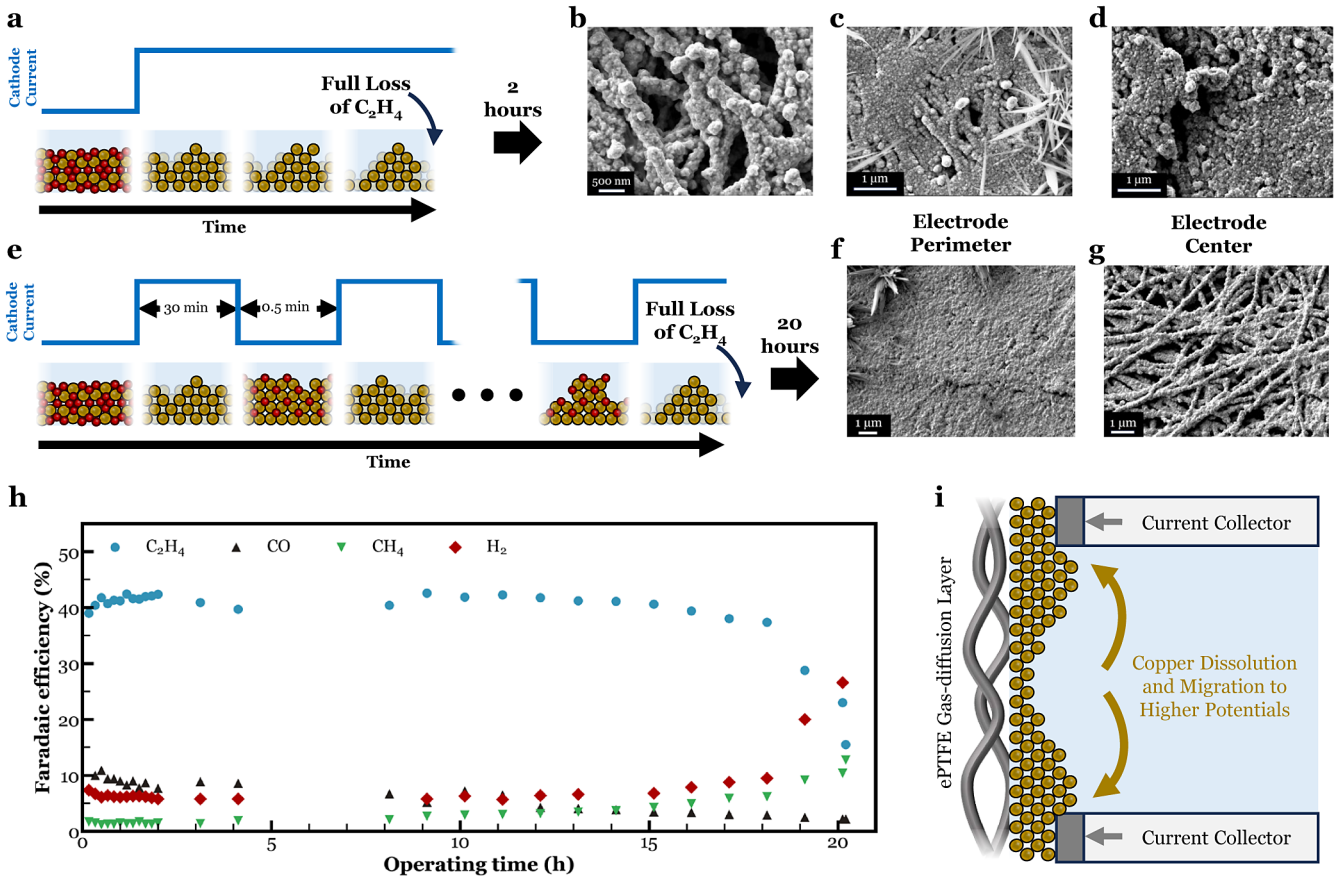

Figure 5. (a) Current profile during a constant chronopotentiometry experiment at −100 mA cm^{-2} along with schematics illustrating the changes in chemical state and morphology at the different stages of the experiment. (b−d) *Ex situ* postmortem SEM images of perimeter (b, 30,000× magnified and c, 25,000× magnified) and center (d, 25,000× magnified) of Cu GDE that was subjected to the current profile in (a). (e) Current profile during pulsed CO_2 electrolysis where a 30-min reductive current at −100 mA cm^{-2} was followed by a 30 s oxidative pulse of 0.524 V *vs* RHE. (f,g) *Ex situ* postmortem SEM images of perimeter (f, 10,000× magnified) and center (g, 13,000× magnified) of Cu GDE that was subjected to the current profile in (d). (h) FE of gas products as a function of operating time during stability test. (i) Schematic illustrating the directional dissolution and migration as a result of the uneven potential distribution.

consumes OH^- ions, the local pH fell back to that of the bulk. With that in mind, during the 30 s "off" time, the catalyst layer could have moved from a condition in which Cu_2O was stable, to metallic Cu being the more stable phase. The likelihood of this happening increases with more cathodic "off" potentials, as these are more near the borders of the Cu/Cu_2O stability regions in the Pourbaix diagram anyway.

The approach of using chronoamperometry to oxidize your catalyst as opposed to chronopotentiometry, with the latter being the most frequently used method in other works, does come with the benefit of controlling your oxidation state more accurately. With chronopotentiometry, the lack of control of potential could result in the (partial) formation of CuO when Cu_2O was the aimed compound.

In order to understand the effect of oxidative pulses on electrochemical surface area (ECSA), we utilized cyclic voltammetry to approximate the ECSA before and after continuous and pulsed electrolysis utilizing electrochemical oxidation. The analysis (Figure S7 and Table S2) shows no significant difference in the change of ECSA over time between the two types of operations, indicating that the observed stability difference is not driven by the surface area of the catalyst.[61]

The Raman data were visualized using a heatmap and are shown in Figure S29. The applied potential is plotted above the heatmap, showing the distinct reduction and oxidation phases.

Stability Test. In the previous sections, pulsed electrolysis, both using chemical oxidation and electrochemical oxidation, was proven to lengthen the catalyst lifetime. Due to the choice of Cu catalyst layer thickness, catholyte pH, and current density, the effects of pulsed electrolysis could already be made visible in a small number of operational hours. In this section, pulsed electrolysis was used to perform a stability test. The changes made to the setup and materials to conduct the stability test are inSupporting Information.

As of all the other results, the outcome of the stability test was compared to the continuous operation case. The current profile of the continuous operation along with the expected change in chemical state and morphology is shown in Figure 5a. SEM images of the perimeter and center of the Cu GDE that was subjected to the current profile in Figure 5a are shown in Figure 5b-d. The GDE's perimeter shows a rougher more agglomerated surface consisting of nanofragments. To further illustrate the potential of maintaining catalyst activity toward C_2H_4, 30 min at −100 mA · cm^{-2} were followed by 30 s of oxidative pulses at 0.524 V *vs* RHE (Figure 5e). The resulting potential curve is shown in Figure S30. And although this approach delays Cu restructuring as Figure 5e suggests, Figure 5f,g still shows restructuring to have occurred. If one compares

https://doi.org/10.1021/jacs.4c06284
J. Am. Chem. Soc. 2024, 146, 19509−19520

the center of the fresh as-sputtered Cu GDE in Figures S1 and 5f, it appears the center orientated copper particles have migrated to the external parts of the electrode, closest to the current collectors (Figure 5i). Literature suggests some dissolution, migration, and deposition occur during operation and in the oxidation/reduction process, resulting in material movement with each cycle.[20,48] This migration of Cu can be overcome or limited through a variety of approaches, which are then expected to extend C_2H_4 further. For example, adding further Cu catalysts would prevent voltage disparities across the electrode,[62] limiting preferential redeposition of Cu to the current collector regions. Additionally, preventing dissolved copper from entering the bulk electrolyte would limit movement per oxidation/reduction cycle. More *ex situ* SEM images are shown in Figure S31. The spatial migration of Cu due to voltage variations is also expected to worsen at elevated current densities as surface voltages would become even more uneven. The effect of aggravated restructuring at elevated current densities on the selectivity curves of CO2RR gas products has been previously and shown in Figure S11. We then stress that overcoming the observed failure mechanism is a first step to identifying and characterizing further mechanisms, and then facilitating higher current density stability tests.

Figure 5h shows the FE curves of the gas products with operating time. The full product distribution was retrieved at three distinguished operational times and can be found in Figure S32, along with a H NMR spectrum of the liquid products found in the catholyte in Figure S33. In the first operating hours, the Cu catalyst became more active toward C_2H_4. Potentially due to an increase in the number of active sites and performing chronopotentiometry at a fixed current density. The optimal current density for C_2H_4 can partially shift over time. After 18 h, the FE of C_2H_4 experiences a firm drop. Within 2 h, the FE of C_2H_4 dropped to 15%. Due to the extent of the restructuring, additional oxidation/reduction cycles would temporarily increase the C_2H_4 selectivity, but this was followed by a significant decay. Hence, it does not allow for the regeneration of the C_2H_4 selectivity back to former values.

With the time dependent selectivity of all gas products as a function of time plotted in Figure 5h, it is noteworthy to mention the decrease in CO production with time. The very same observation was made for the previously 3-h electrochemical pulsed operation tests as well. The steady decrease in CO could indicate a decrease in CO_2 to CO catalytic sites, that then eventually shuts down C_2-hydrocarbon production. Similarly, as CO decreases, H_2 and CH_4 increase, potentially implying that additional sites begin to favor these products. Previous works, for example, have shown that high or low ratios of Cu(100) to Cu(111) will promote C_2H_4 or CH_4 and H_2 formation, respectively, and the site distribution is known to change over time.[49] Tracking products, like CO, may then also be used to detect early failure of the Cu catalyst. With lab tests moving into the 100s or 1000s hour range, such methodologies for early detection are important to increase throughput.

CONCLUSION

The sustainable production of C_2 hydrocarbons through CO_2 electrolysis suffers from stability issues as Cu reconstructs and deactivates under a negative applied potential. In this work, we provided a deeper understanding of the chemical processes that occur during both chemical oxidation and electrochemical oxidation during pulsed electrolysis as a method to increase the lifetime of Cu catalysts for CO2RR. Specific system design choices allowed for a low number of operational hours to be sufficient for the study of the catalyst degradation. By varying the "off" time, the chemical oxidation of Cu to Cu_2O was found to be kinetically limited by the oxygen flux to the cathode. This was confirmed by *in situ* Raman spectroscopy. Lengthening the catalyst lifetime using electrochemical oxidation was largely dependent on the programmed "off" potential. Here, the chosen "off" potentials, although only 10 mV apart, resulted in very different ethylene selectivity trends as a function of time. Although the closure of the electrochemical circuit during electrochemical oxidation changes the number of reactions involved, for both chemical and electrochemical oxidation it is the total reactivated area that is believed to play a key role in lengthening the catalyst lifetime. A stability test with implemented electrochemical oxidation periods achieved a stable FE of C_2H_4 of ∼38% for 18 h of operation. It appeared from the SEM images that the high number of oxidation/reduction cycles resulted in a large number of copper fragments dissolving and redepositing on the sides of the GDE. Looking into strategies to minimize this process is believed to hold great value for lengthening copper lifetimes during both pulsed and constant electrolysis.

ASSOCIATED CONTENT

Data Availability Statement

All data are made available in the manuscript and the Supporting Information. Raw data made available through deposition on the 4TU.Centre.

Supporting Information

The Supporting Information is available free of charge at https://pubs.acs.org/doi/10.1021/jacs.4c06284.

Details on the setup and materials used, SEM images, full product distribution of the stability test, Faradaic efficiency plots of all gas products, EDS data (PDF)

AUTHOR INFORMATION

Corresponding Author

Thomas Burdyny − *Materials for Energy Conversion and Storage (MECS), Department of Chemical Engineering, Faculty of Applied Sciences, Delft University of Technology, Delft 2629 HZ, The Netherlands;* orcid.org/0000-0001-8057-9558; Email: T.E.Burdyny@tudelft.nl

Authors

Jesse Kok − *Materials for Energy Conversion and Storage (MECS), Department of Chemical Engineering, Faculty of Applied Sciences, Delft University of Technology, Delft 2629 HZ, The Netherlands*

Jim de Ruiter − *Inorganic Chemistry and Catalysis, Debye Institute for Nanomaterials Science & Institute for Sustainable and Circular Chemistry, Utrecht University, Utrecht 3584 CG, The Netherlands*

Ward van der Stam − *Inorganic Chemistry and Catalysis, Debye Institute for Nanomaterials Science & Institute for Sustainable and Circular Chemistry, Utrecht University, Utrecht 3584 CG, The Netherlands;* orcid.org/0000-0001-8155-5400

Complete contact information is available at: https://pubs.acs.org/10.1021/jacs.4c06284

Notes

The authors declare no competing financial interest.

■ ACKNOWLEDGMENTS

The authors would like to acknowledge the NWO for providing the FlexEChem Grant (NWA.1237.18.002) *via* the NWA-themed call "Opslag en conversie". Furthermore, the authors would like to thank Siddhartha Subramanian, Pranav Karanth, and Arij Makhzoum for the SEM images and the results displayed in Figures S10 and S11.

■ REFERENCES

(1) Okoye-Chine, C. G.; Otun, K.; Shiba, N.; Rashama, C.; Ugwu, S. N.; Onyeaka, H.; Okeke, C. T. Conversion of Carbon Dioxide into Fuels—A Review. *J. CO2 Util.* **2022**, *62*, 102099.
(2) Billy, J. T.; Co, A. C. Experimental Parameters Influencing Hydrocarbon Selectivity during the Electrochemical Conversion of CO $_2$. *ACS Catal.* **2017**, *7* (12), 8467−8479.
(3) *Modern Aspects of Electrochemistry*, Vayenas, C. G.; White, R. E.; Gamboa-Aldeco, M. E.; Springer New York: New York, NY, 2008; Vol. *42*. DOI: .
(4) Sassenburg, M.; De Rooij, R.; Nesbitt, N. T.; Kas, R.; Chandrashekar, S.; Firet, N. J.; Yang, K.; Liu, K.; Blommaert, M. A.; Kolen, M.; Ripepi, D.; Smith, W. A.; Burdyny, T. Characterizing CO $_2$ Reduction Catalysts on Gas Diffusion Electrodes: Comparing Activity, Selectivity, and Stability of Transition Metal Catalysts. *ACS Appl. Energy Mater.* **2022**, *5* (5), 5983−5994.
(5) Hori, Y.; Murata, A.; Takahashi, R. Formation of Hydrocarbons in the Electrochemical Reduction of Carbon Dioxide at a Copper Electrode in Aqueous Solution. *J. Chem. Soc., Faraday Trans. 1* **1989**, *85* (8), 2309.
(6) Gonçalves, M. R.; Gomes, A.; Condeço, J.; Fernandes, T. R. C.; Pardal, T.; Sequeira, C. A. C.; Branco, J. B. Electrochemical Conversion of CO2 to C2 Hydrocarbons Using Different Ex Situ Copper Electrodeposits. *Electrochim. Acta* **2013**, *102*, 388−392.
(7) Kibria, M. G.; Edwards, J. P.; Gabardo, C. M.; Dinh, C.; Seifitokaldani, A.; Sinton, D.; Sargent, E. H. Electrochemical Co2 Reduction into Chemical Feedstocks: From Mechanistic Electrocatalysis Models to System Design. *Adv. Mater* **2019**, *31*, 31.
(8) Ren, D.; Deng, Y.; Handoko, A. D.; Chen, C. S.; Malkhandi, S.; Yeo, B. S. Selective Electrochemical Reduction of Carbon Dioxide to Ethylene and Ethanol on Copper(I) Oxide Catalysts. *ACS Catal.* **2015**, *5* (5), 2814−2821.
(9) Heenen, H. H.; Shin, H.; Kastlunger, G.; Overa, S.; Gauthier, J. A.; Jiao, F.; Chan, K. The Mechanism for Acetate Formation in Electrochemical CO $_{(2)}$ Reduction on Cu: Selectivity with Potential, pH, and Nanostructuring. *Energy Environ. Sci.* **2022**, *15* (9), 3978−3990.
(10) Chen, C.; Li, Y.; Yu, S.; Louisia, S.; Jin, J.; Li, M.; Ross, M. B.; Yang, P. Cu-Ag Tandem Catalysts for High-Rate CO2 Electrolysis toward Multicarbons. *Joule* **2020**, *4* (8), 1688−1699.
(11) García De Arquer, F. P.; Dinh, C.-T.; Ozden, A.; Wicks, J.; McCallum, C.; Kirmani, A. R.; Nam, D.-H.; Gabardo, C.; Seifitokaldani, A.; Wang, X.; Li, Y. C.; Li, F.; Edwards, J.; Richter, L. J.; Thorpe, S. J.; Sinton, D.; Sargent, E. H. CO $_2$ Electrolysis to Multicarbon Products at Activities Greater than 1 A Cm $^{-2}$. *Science* **2020**, *367* (6478), 661−666.
(12) Burdyny, T.; Smith, W. A. CO $_2$ Reduction on Gas-Diffusion Electrodes and Why Catalytic Performance Must Be Assessed at Commercially-Relevant Conditions. *Energy Environ. Sci.* **2019**, *12* (5), 1442−1453.
(13) Nguyen, T. N.; Dinh, C.-T. Gas Diffusion Electrode Design for Electrochemical Carbon Dioxide Reduction. *Chem. Soc. Rev.* **2020**, *49* (21), 7488−7504.
(14) Gabardo, C. M.; O'Brien, C. P.; Edwards, J. P.; McCallum, C.; Xu, Y.; Dinh, C.-T.; Li, J.; Sargent, E. H.; Sinton, D. Continuous Carbon Dioxide Electroreduction to Concentrated Multi-Carbon Products Using a Membrane Electrode Assembly. *Joule* **2019**, *3* (11), 2777−2791.
(15) Schreiber, M. W. Industrial CO2 Electroreduction to Ethylene: Main Technical Challenges. *Curr. Opin. Electrochem.* **2024**, *44*, 101438.
(16) Jung, H.; Lee, S. Y.; Lee, C. W.; Cho, M. K.; Won, D. H.; Kim, C.; Oh, H.-S.; Min, B. K.; Hwang, Y. J. Electrochemical Fragmentation of Cu $_2$ O Nanoparticles Enhancing Selective C−C Coupling from CO $_2$ Reduction Reaction. *J. Am. Chem. Soc.* **2019**, *141* (11), 4624−4633.
(17) Galeano, C.; Meier, J. C.; Peinecke, V.; Bongard, H.; Katsounaros, I.; Topalov, A. A.; Lu, A.; Mayrhofer, K. J. J.; Schüth, F. Toward Highly Stable Electrocatalysts via Nanoparticle Pore Confinement. *J. Am. Chem. Soc.* **2012**, *134* (50), 20457−20465.
(18) Simon, G. H.; Kley, C. S.; Roldan Cuenya, B. Potential-Dependent Morphology of Copper Catalysts During CO_2 Electroreduction Revealed by In Situ Atomic Force Microscopy. *Angew. Chem., Int. Ed.* **2021**, *60* (5), 2561−2568.
(19) Clark, E. L.; Resasco, J.; Landers, A.; Lin, J.; Chung, L.-T.; Walton, A.; Hahn, C.; Jaramillo, T. F.; Bell, A. T. Standards and Protocols for Data Acquisition and Reporting for Studies of the Electrochemical Reduction of Carbon Dioxide. *ACS Catal.* **2018**, *8* (7), 6560−6570.
(20) Raaijman, S. J.; Arulmozhi, N.; Koper, M. T. M. Morphological Stability of Copper Surfaces under Reducing Conditions. *ACS Appl. Mater. Interfaces* **2021**, *13* (41), 48730−48744.
(21) Yang, K.; Kas, R.; Smith, W. A.; Burdyny, T. Role of the Carbon-Based Gas Diffusion Layer on Flooding in a Gas Diffusion Electrode Cell for Electrochemical CO $_2$ Reduction. *ACS Energy Lett.* **2021**, *6* (1), 33−40.
(22) Garg, S.; Xu, Q.; Moss, A. B.; Mirolo, M.; Deng, W.; Chorkendorff, I.; Drnec, J.; Seger, B. How Alkali Cations Affect Salt Precipitation and CO $_2$ Electrolysis Performance in Membrane Electrode Assembly Electrolyzers. *Energy Environ. Sci.* **2023**, *16* (4), 1631−1643.
(23) Vavra, J.; Shen, T.; Stoian, D.; Tileli, V.; Buonsanti, R. Real-time Monitoring Reveals Dissolution/Redeposition Mechanism in Copper Nanocatalysts during the Initial Stages of the CO $_2$ Reduction Reaction. *Angew. Chem.* **2021**, *133* (3), 1367−1374.
(24) Vavra, J.; Ramona, G. P. L.; Dattila, F.; Kormányos, A.; Priamushko, T.; Albertini, P. P.; Loiudice, A.; Cherevko, S.; Lopéz, N.; Buonsanti, R. Solution-Based Cu+ Transient Species Mediate the Reconstruction of Copper Electrocatalysts for CO2 Reduction. *Nat. Catal.* **2024**, *7*, 89.
(25) Drisdell, W.; Lee, S. H.; Acosta, J. A.; Lee, D.; Larson, D.; Li, H.; Chen, J.; Blair, S.; Gallo, A.; Zheng, H.; Tassone, C.; Jaramillo, T. Structural Transformation and Degradation of Cu Nanocatalysts during Electrochemical CO2 Reduction Reaction, 2023. . preprint; In Review.
(26) Amirbeigiarab, R.; Tian, J.; Herzog, A.; Qiu, C.; Bergmann, A.; Roldan Cuenya, B.; Magnussen, O. M. Atomic-Scale Surface Restructuring of Copper Electrodes under CO2 Electroreduction Conditions. *Nat. Catal.* **2023**, *6* (9), 837−846.
(27) Jiang, S.; D'Amario, L.; Dau, H. Copper Carbonate Hydroxide as Precursor of Interfacial CO in CO $_2$ Electroreduction. *ChemSuschem* **2022**, *15* (8), No. e202102506.
(28) An, H.; Wu, L.; Gijsberg, Z.; Yang, S.; Hartman, T.; Weckhuysen, B. M.; Van Der Stam, W. Probing the Dynamics of Low-Overpotential CO $_2$ -to-CO Activation on Copper Electrodes with Time-Resolved Raman Spectroscopy. *J. Am. Chem. Soc.* **2022**, *144* (33), 15047−15058.
(29) Popovic, S.; Bele, M.; Hodnik, N. Reconstruction of Copper Nanoparticles at Electrochemical CO $_2$ Reduction Reaction Conditions Occurs *via* Two-step Dissolution/Redeposition Mechanism. *ChemElectrochem* **2021**, *8* (14), 2634−2639.
(30) Lai, W.; Ma, Z.; Zhang, J.; Yuan, Y.; Qiao, Y.; Huang, H. Dynamic Evolution of Active Sites in Electrocatalytic CO $_2$ Reduction Reaction: Fundamental Understanding and Recent Progress. *Adv. Funct. Mater.* **2022**, *32* (16), 2111193.

(31) Zhao, Y.; Chang, X.; Malkani, A. S.; Yang, X.; Thompson, L.; Jiao, F.; Xu, B.Speciation of Cu Surfaces During the Electrochemical CO Reduction ReactionJ. *Am. Chem. Soc.***2020**14297359743
(32) Cherevko, S.; Zeradjanin, A. R.; Topalov, A. A.; Kulyk, N.; Katsounaros, I.; Mayrhofer, K. J. J. Dissolution of Noble Metals during Oxygen Evolution in Acidic Media. *ChemCatchem* **2014**, *6* (8), 2219−2223.
(33) Liu, Q.; Jiang, Q.; Li, L.; Yang, W. Spontaneous Reconstruction of Copper Active Sites during the Alkaline CORR: Degradation and Recovery of the Performance. *J. Am. Chem. Soc.* **2024**, *146*, 4242−4251.
(34) Hori, Y.; Konishi, H.; Futamura, T.; Murata, A.; Koga, O.; Sakurai, H.; Oguma, K. Deactivation of Copper Electrode" in Electrochemical Reduction of CO2. *Electrochim. Acta* **2005**, *50* (27), 5354−5369.
(35) Wuttig, A.; Surendranath, Y. Impurity Ion Complexation Enhances Carbon Dioxide Reduction Catalysis. *ACS Catal.* **2015**, *5* (7), 4479−4484.
(36) Obasanjo, C. A.; Zeraati, A. S.; Shiran, H. S.; Nguyen, T. N.; Sadaf, S. M.; Kibria, M. G.; Dinh, C.-T. *In Situ* Regeneration of Copper Catalysts for Long-Term Electrochemical CO_2 Reduction to Multiple Carbon Products. *J. Mater. Chem. A* **2022**, *10* (37), 20059−20070.
(37) Nguyen, T. N.; Chen, Z.; Zeraati, A. S.; Shiran, H. S.; Sadaf, S.; Kibria, M. G.; Sargent, E. H.; Dinh, C.-T. Catalyst Regeneration via Chemical Oxidation Enables Long-Term Electrochemical Carbon Dioxide Reduction. *J. Am. Chem. Soc.* **2022**, *144* (29), 13254−13265.
(38) Jännsch, Y.; Leung, J. J.; Hämmerle, M.; Magori, E.; Wiesner-Fleischer, K.; Simon, E.; Fleischer, M.; Moos, R. Pulsed Potential Electrochemical CO2 Reduction for Enhanced Stability and Catalyst Reactivation of Copper Electrodes. *Electrochem. Commun.* **2020**, *121*, 106861.
(39) Bui, J. C.; Kim, C.; Weber, A. Z.; Bell, A. T. Dynamic Boundary Layer Simulation of Pulsed CO_2 Electrolysis on a Copper Catalyst. *ACS Energy Lett.* **2021**, 1181−1188.
(40) Tang, Z.; Nishiwaki, E.; Fritz, K. E.; Hanrath, T.; Suntivich, J. Cu(I) Reducibility Controls Ethylene vs Ethanol Selectivity on (100)-Textured Copper during Pulsed CO_2 Reduction. *ACS Appl. Mater. Interfaces* **2021**, *13* (12), 14050−14055.
(41) Xiao, H.; Goddard, W. A.; Cheng, T.; Liu, Y. Cu Metal Embedded in Oxidized Matrix Catalyst to Promote CO_2 Activation and CO Dimerization for Electrochemical Reduction of CO_2. *Proc. Natl. Acad. Sci. U. S. A.* **2017**, *114* (26), 6685−6688.
(42) Wang, S.; Kou, T.; Baker, S. E.; Duoss, E. B.; Li, Y. Recent Progress in Electrochemical Reduction of CO2 by Oxide-Derived Copper Catalysts. *Materials Today Nano* **2020**, *12*, 100096.
(43) Lei, Q.; Zhu, H.; Song, K.; Wei, N.; Liu, L.; Zhang, D.; Yin, J.; Dong, X.; Yao, K.; Wang, N.; Li, X.; Davaasuren, B.; Wang, J.; Han, Y. Investigating the Origin of Enhanced C_{2+} Selectivity in Oxide-/Hydroxide-Derived Copper Electrodes during CO_2 Electroreduction. *J. Am. Chem. Soc.* **2020**, *142* (9), 4213−4222.
(44) Scholten, F.; Nguyen, K. C.; Bruce, J. P.; Heyde, M.; Roldan Cuenya, B. Identifying Structure−Selectivity Correlations in the Electrochemical Reduction of CO_2: A Comparison of Well-Ordered Atomically Clean and Chemically Etched Copper Single-Crystal Surfaces. *Angew. Chem., Int. Ed.* **2021**, *60* (35), 19169−19175.
(45) Zhu, C.; Zhang, Z.; Zhong, L.; Hsu, C.-S.; Xu, X.; Li, Y.; Zhao, S.; Chen, S.; Yu, J.; Chen, S.; Yu, J.; Chen, S.; Wu, M.; Gao, P.; Li, S.; Chen, H. M.; Liu, K.; Zhang, L. Product-Specific Active Site Motifs of Cu for Electrochemical CO_2 Reduction. *Chem* **2021**, *7* (2), 406−420.
(46) Speck, F. D.; Zagalskaya, A.; Alexandrov, V.; Cherevko, S. Periodicity in the Electrochemical Dissolution of Transition Metals. *Angew. Chem., Int. Ed.* **2021**, *60* (24), 13343−13349.
(47) Zhong, D.; Cheng, D.; Fang, Q.; Liu, Y.; Li, J.; Zhao, Q. Understanding the Restructuring and Degradation of Oxide-Derived Copper during Electrochemical CO2 Reduction. *Chem. Eng. J.* **2023**, *470*, 143907.
(48) Speck, F. D.; Cherevko, S. Electrochemical Copper Dissolution: A Benchmark for Stable CO2 Reduction on Copper Electrocatalysts. *Electrochem. Commun.* **2020**, *115*, 106739.
(49) De Gregorio, G. L.; Burdyny, T.; Loiudice, A.; Iyengar, P.; Smith, W. A.; Buonsanti, R. Facet-Dependent Selectivity of Cu Catalysts in Electrochemical CO_2 Reduction at Commercially Viable Current Densities. *ACS Catal.* **2020**, *10* (9), 4854−4862.
(50) Kortlever, R.; Shen, J.; Schouten, K. J. P.; Calle-Vallejo, F.; Koper, M. T. M. Catalysts and Reaction Pathways for the Electrochemical Reduction of Carbon Dioxide. *J. Phys. Chem. Lett.* **2015**, *6* (20), 4073−4082.
(51) Pourbaix, M. Applications of Electrochemistry in Corrosion Science and in Practice. *Corros. Sci.* **1974**, *14* (1), 25−82.
(52) Lee, S. Y.; Jung, H.; Kim, N.-K.; Oh, H.-S.; Min, B. K.; Hwang, Y. J. Mixed Copper States in Anodized Cu Electrocatalyst for Stable and Selective Ethylene Production from CO_2 Reduction. *J. Am. Chem. Soc.* **2018**, *140* (28), 8681−8689.
(53) Zhang, Z.; Dua, R.; Zhang, L.; Zhu, H.; Zhang, H.; Wang, P. Carbon-Layer-Protected Cuprous Oxide Nanowire Arrays for Efficient Water Reduction. *ACS Nano* **2013**, *7* (2), 1709−1717.
(54) El Din, A. M. S.; El Wahab, F. M. A. The Behaviour of the Copper Electrode in Alkaline Solutions upon Alternate Anodic and Cathodic Polarization. *Electrochim. Acta* **1964**, *9* (1), 113−121.
(55) Yang, Y.; Han, J.; Ning, X.; Su, J.; Shi, J.; Cao, W.; Xu, W. Photoelectrochemical Stability Improvement of Cuprous Oxide (Cu_2O) Thin Films in Aqueous Solution: Photoelectrochemical Stability Improvement of Cu_2O in Aqueous Solution. *Int. J. Energy Res.* **2016**, *40* (1), 112−123.
(56) Atkins, P. W.; de Paula, J.; Keeler, J. *Physical Chemistry*, 11 th ed.; Oxford University Press, 2018.
(57) Pedeferri, P. *Corrosion Science and Engineering; Engineering Materials*; Springer International Publishing: Cham, 2018. .
(58) McCafferty, E. *Introduction to Corrosion Science*; Springer New York: New York, NY, 2010. DOI: .
(59) Sauvé, E. R.; Tang, B. Y.; Razdan, N. K.; Toh, W. L.; Weng, S.; Surendranath, Y. Open Circuit Potential Decay Transients Quantify Interfacial pH Swings during High Current Density Hydrogen Electrocatalysis. *Joule* **2024**, *8*, 728−745.
(60) Bard, A. J.; Faulkner, L. R. *Electrochemical Methods: Fundamentals and Applications*, 2nd ed.; nd ed.; Wiley: New York Weinheim, 2001.
(61) Arán-Ais, R. M.; Scholten, F.; Kunze, S.; Rizo, R.; Roldan Cuenya, B. The Role of in Situ Generated Morphological Motifs and Cu(i) Species in C2+ Product Selectivity during CO_2 Pulsed Electroreduction. *Nat. Energy* **2020**, *5* (4), 317−325.
(62) Iglesias Van Montfort, H.-P.; Li, M.; Irtem, E.; Abdinejad, M.; Wu, Y.; Pal, S. K.; Sassenburg, M.; Ripepi, D.; Subramanian, S.; Biemolt, J.; Rufford, T. E.; Burdyny, T. Non-Invasive Current Collectors for Improved Current-Density Distribution during CO_2 Electrolysis on Super-Hydrophobic Electrodes. *Nat. Commun.* **2023**, *14* (1), 6579.